# Angles Only Initial Orbit Determination: Comparison of Relative Dynamics and Inertial Dynamics Approaches with Error Analysis

T. Alan Lovell[1]
*Air Force Research Laboratory, Kirtland AFB, NM, USA*

Kenneth R. Horneman[2]
*National Research Council, Washington, DC, USA*

Alex E. Sizemore[3]
*University of Kansas, Lawrence, KS, USA*

and
Bradyn W. Morton[4]
*Missouri University of Science and Technology, Rolla, MO, USA*

**This paper investigates methods based on relative orbital dynamics to determine the motion of a space object using line-of-sight measurements collected by a space-based observer. The so-called "initial relative orbit determination" methods are typically applied to scenarios involving close proximity between the observer and the space object, i.e. scenarios in which the observer and space object are in very similar orbits. However, these methods are mathematically applicable to larger separation scenarios in which the observer and space object are in very different orbits. Previous work demonstrated an initial relative orbit determination algorithm that incorporates a closed-form relative motion solution with second-order accuracy. This paper introduces a similar algorithm incorporating a third-order solution and compares its performance to the second-order method over various simulated test cases involving different observer-object scenarios. In particular, the sensitivity of these algorithms to measurement error and measurement sample rate is explored.**

## I. Introduction

Angles-only initial orbit determination (IOD) enables the determination of a space object's orbit about a central body using a minimal number of line-of-sight (LOS) measurements, where the location of the observer at each measurement time is assumed known. This astrodynamics problem has been explored for many years, but is still a subject of ongoing research. The Gauss and Laplace methods are examples of classical IOD techniques (see, for example, Refs 1-3). These methods are based on the inertial dynamics of the space object (typically from a two-body gravitational perspective) and only require the LOS measurements and the observer location at each measurement time as inputs.

Recently, the growth of spacecraft missions involving formation flying, rendezvous, and proximity operations has motivated the study of angles-only IOD techniques based on the relative dynamics between the observer (or some reference orbit) and the space object. We will use the term initial relative orbit determination (IROD) to refer to these techniques. The relative approach allows the use of closed-form approximate solutions of the relative motion dynamics, such as linear or second-order models (e.g. Refs 4-8). This in turn allows the possibility of an IROD algorithm that, if not entirely closed-form, at least exhibits compactness and involves little to no iteration. Like the classical IOD methods, the IROD algorithms only require LOS measurements and observer location at each measurement time, although this data is typically expressed in the local-vertical local-horizontal (LVLH) frame of the observer. Some initial studies involving IROD algorithms include Refs 9-10.

---

[1] Senior Aerospace Engineer, Space Vehicles Directorate, Associate Fellow AIAA.
[2] Postdoctoral Research Associate, Member AIAA.
[3] Graduate Student, Dept of Aerospace Engineering, Member AIAA.
[4] Graduate Student, Dept of Aerospace Engineering, Member AIAA.

IROD algorithms were initially designed for close-proximity scenarios. One such type of scenario involves rendezvous and proximity operations, whereby the observer performs passive "relative navigation" with a space object for purposes of circumnavigation, inspection, etc. Another type of scenario involves relative navigation among the members of a satellite formation, in which information between members can be cooperatively exchanged. However, IROD algorithms can be applied outside of this regime, i.e. between an observer and object that are not necessarily close. We will refer to these types of scenarios as space-based space situational awareness (SBSSA). One SBSSA application involves the observer finding an object in its field of view whose orbit is unknown. If the observer captures several images of the object and converts the images to LOS vectors, IOD algorithms (of either the classical or IROD variety) can be applied to the data to obtain an initial orbit estimate for the object. It should be mentioned that the conversion of image data to LOS data is nontrivial, particularly if the object is far enough away that it blends in with the star background. For this paper, it will be assumed that the necessary image processing techniques are available to perform this step, and also that the necessary information (e.g. observer orbit knowledge) is available to express the LOS vectors in the observer's LVLH frame. Thus, the inputs to the IROD algorithms are LOS vectors expressed in LVLH.

This paper will investigate IOD from an SBSSA perspective. Previous work (Ref 11) demonstrated an IROD algorithm that incorporates a closed-form relative motion solution expanded to second order in the initial conditions. This paper introduces a similar algorithm incorporating a third-order solution and compares its performance to the second-order method over various simulated test cases involving different observer and object orbits. First, relative motion dynamics is briefly reviewed, with a description of the second- and third-order solutions. The IROD technique is then conceptually described, and the test cases are defined. The "angle error" metric is then defined and explored for linear, second-order, and third-order solutions. Finally, the performance of the second- and third-order IROD methods is demonstrated for the test cases. In particular, the sensitivity of these algorithms to measurement error and measurement sample rate is detailed.

.

## II. Relative Motion Dynamics

Before introducing the IROD method, a brief discussion of relative motion dynamics is in order, including certain closed-form relative motion solutions that exist. An effective coordinate frame in which to characterize the motion of a "deputy" space object relative to a "chief" object is a Cartesian coordinate frame known as the local-vertical-local-horizontal (LVLH) frame. This frame entails defining a reference orbit about the Earth, defining the chief object on this orbit, and attaching a coordinate frame to the chief's center of mass. This is depicted in Figure 1. The LVLH coordinate directions are then defined as follows: the "x" or radial direction is aligned with the chief's inertial position vector (i.e. the vector from Earth's center to the chief), the "z" or cross-track direction is aligned with the chief's angular momentum vector (i.e. perpendicular to the chief's orbit plane), and the "y" direction is the cross product of z and x. (If the chief orbit is circular, the "y" direction is then aligned with the chief's inertial velocity vector and is often called along-track.) Note that the LVLH frame translates and rotates around the Earth with the chief object, therefore these directions are defined instantaneously. In this paper, we model the relative motion between the observer and a resident space object (RSO) in this frame.

Probably the most well-known closed-form solution for relative motion is that of Clohessy and Wiltshire.[5] This solution assumes the chief orbit is circular and is commonly derived by writing the two-body ordinary differential equations (ODEs) of motion for both the chief and deputy, differencing these equations, and expanding the differenced to first order in a Taylor series. The result is a set of linear time-invariant ODEs in LVLH coordinates, whose solution is easily obtained and takes the form of a linear combination of the relative initial conditions. Other authors[6-8] have expanded the differenced ODEs to second order and derived an approximate solution to the ODEs. This solution contains not only the first-order terms of the Clohessy-Wiltshire solution, but second-order terms in the relative initial conditions as well. Finally, Ref. 12 derives a closed-form relative motion solution containing terms up to third order. All of these solutions are represented by the comprehensive solution given in the Appendix, whereby the linear (Clohessy-Wiltshire) solution contains only the terms with $a_i$ coefficents, the second-order solution contains the terms with $a_i$ and $b_i$ coefficents, and the third-order solution contains the terms with $a_i$, $b_i$, and $c_i$ coefficents.

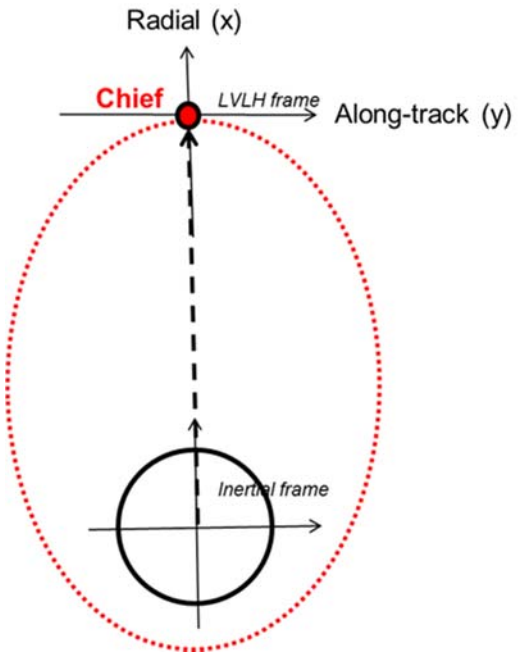


**Figure 1. LVLH coordinate frame, with chief orbit and x and y axis directions depicted, and z axis direction going into the page.**

## III. Initial Relative Orbit Determination

In this section, the concept of LOS (or angles-only) initial relative orbit determination is described. The LOS measurement equations are first derived, followed by a discussion of the observability issue arising in space-based OD scenarios, then a candidate IROD algorithm is laid out.

### A. Derivation of Measurement Equations

Consider a measured LOS vector at time $t_i$ expressed in the LVLH frame, i.e. $\hat{u}_r(t_i) = u_x(t_i)\hat{i} + u_y(t_i)\hat{j} + u_z(t_i)\hat{k}$. The measurement equations can be formed by requiring that the relative position vector is parallel to the LOS at each measurement time:

$$\hat{u}_r(t_i) \times \bar{r}(t_i) = U(t_i)\bar{r}(t_i) = \begin{bmatrix} 0 & -u_z(t_i) & u_y(t_i) \\ u_z(t_i) & 0 & -u_x(t_i) \\ -u_y(t_i) & u_x(t_i) & 0 \end{bmatrix} \bar{r}(t_i) = 0 \tag{1}$$

or

$$\begin{aligned} u_z(t_i)y(t_i) - u_y(t_i)z(t_i) &= 0 \\ u_z(t_i)x(t_i) - u_x(t_i)z(t_i) &= 0 \\ u_y(t_i)x(t_i) - u_x(t_i)y(t_i) &= 0 \end{aligned} \tag{2}$$

Note that the LOS components $u_x(t_i)$, $u_y(t_i)$, $u_z(t_i)$ are known, but the relative position states $x(t_i)$, $y(t_i)$, $z(t_i)$ are unknown. The relative position states at $t_i$ can be related to the initial relative states $\begin{bmatrix} x_0 & y_0 & z_0 & \dot{x}_0 & \dot{y}_0 & \dot{z}_0 \end{bmatrix}^T$ via a closed-form relative motion solution (e.g. one of the solutions cited above). This would yield three equations whose unknowns are the initial relative states. However, only two of the three equations in Eq. (2) are independent. Thus, if we obtain

a LOS measurement at three specific times, choose two of the equations from Eq. (2) at each time, and employ a closed-form relative motion solution, we have a "square" system, i.e. six measurement equations from which to solve the six initial relative states $\left[x_0 \;\; y_0 \;\; z_0 \;\; \dot{x}_0 \;\; \dot{y}_0 \;\; \dot{z}_0\right]^T$.

**B. Observability**

Suppose we follow the above procedure and choose as our closed-form relative motion solution a linear solution such as the Clohessy-Wiltshire solution. We can then write the solution in the form of a state-transition matrix $\Phi(t_i, t_0)$ and can relate the relative position vector at $t_i$ to the initial state vector using elements of the state-transition matrix:

$$\bar{r}(t_i) = \left[x(t_i) \quad y(t_i) \quad z(t_i)\right]^T = \left[\Phi_{rr}(t_i, t_0) \quad \Phi_{rv}(t_i, t_0)\right]\bar{x}_0 \tag{3}$$

where $\bar{x}_0$ represents the six initial relative states $\left[x_0 \;\; y_0 \;\; z_0 \;\; \dot{x}_0 \;\; \dot{y}_0 \;\; \dot{z}_0\right]^T$ and $\Phi_{rr}(t_i, t_0)$ and $\Phi_{rv}(t_i, t_0)$ represent the upper left and upper right 3x3 submatrices of $\Phi(t_i, t_0)$, respectively. Inserting Eq. (3) into Eq. (1) yields

$$\begin{bmatrix} 0 & -u_z(t_i) & u_y(t_i) \\ u_z(t_i) & 0 & -u_x(t_i) \\ -u_y(t_i) & u_x(t_i) & 0 \end{bmatrix}\left[\Phi_{rr}(t_i, t_0) \quad \Phi_{rv}(t_i, t_0)\right]\bar{x}_0 = 0 \tag{4}$$

These are linear equations in $\bar{x}_0$. Again, only two of the three equations are independent, so if we obtain three LOS measurements, choosing two of the measurement equations at each time, this yields a system of the form $A\bar{x}_0 = 0$, where $A$ is a 6x6 matrix whose elements are known.

If there exists a nonzero solution $\bar{x}_0^*$ to this system, then $\alpha\bar{x}_0^*$ is a solution as well, where $\alpha$ is any positive real value. This implies an infinite number of relative orbits corresponding to a given set of LOS measurements; in fact, these relative orbits don't just possess the same LOS values at specific measurement times, but in fact for all time. Physically, this can be thought of as "range ambiguity," as depicted in Figure 2 (where the Clohessy-Wiltshire solution is used to propagate the relative motion). Each plot shows a manifold or "family" of multiple trajectories possessing an initial state of the form $\alpha\bar{x}_0^*$. For each manifold, the trajectories share the same $\bar{x}_0^*$, but each trajectory corresponds to a different value of $\alpha$. From an IROD perspective, it is possible that in a particular scenario $\bar{x}_0^*$ can be determined, but the specific "size" or scale factor $\alpha$ of the trajectory cannot be determined. This scenario of guaranteed infinite ambiguity will be referred to as "Woffinden's Dilemma" because it was first described in Ref 13. Note that this guaranteed ambiguity is not a function of how many measurements are taken; i.e., one cannot somehow create observability by taking more measurements.

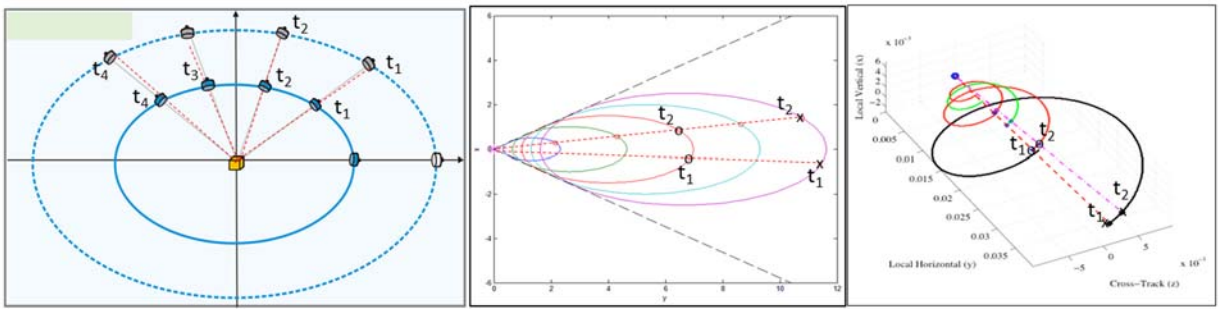


**Figure 2. Representation of a "family" of ambiguous relative orbits, as seen by a space-based observer (Figure 2a: circumnavigation orbits, Figure 2b: offset orbits, Figure 2c: 3-D drifting orbits).**

Obviously, actual relative motion between space objects is not linear. In reality, if one were to construct a "family" of relative orbits whose states at a particular time were all scale mutliples of one another (i.e. each orbit corresponding to a particular $\alpha$), the relative orbits would have similar, but not identical, LOS histories. This is illustrated in Figure 3, whereby two relative orbits whose initial conditions are scale multiples of each other are propagated forward with nonlinear dynamics. It is seen that the LOS histories of the two trajectories are not identical, as would be predicted by linear dynamics, but in fact deviate increasingly over time. The members of this hypothetical family of relative orbits that are closer to the observer (where "closer" implies smaller values of the relative states) would have LOS histories closer to that predicted by linear dynamics, whereas the farther from the observer a particular family member is (i.e. the larger the relative orbit), the more its LOS history will deviate from the linear model. It is the authors' general contention that the amount of deviation, or dis-similarity, in a relative orbit compared to that predicted by linear dynamics is correlated with the degree of nonlinearity in the orbit, and correspondingly the degree of observability. That is, the closer a particular relative motion scenario is to linear behavior (i.e. the less separation or difference between the observer and RSO orbits), the weaker the observability and the more difficult it is to determine the unique relative orbit (particularly its "size" or scale factor). Conversely, larger relative orbits will possess higher observability.

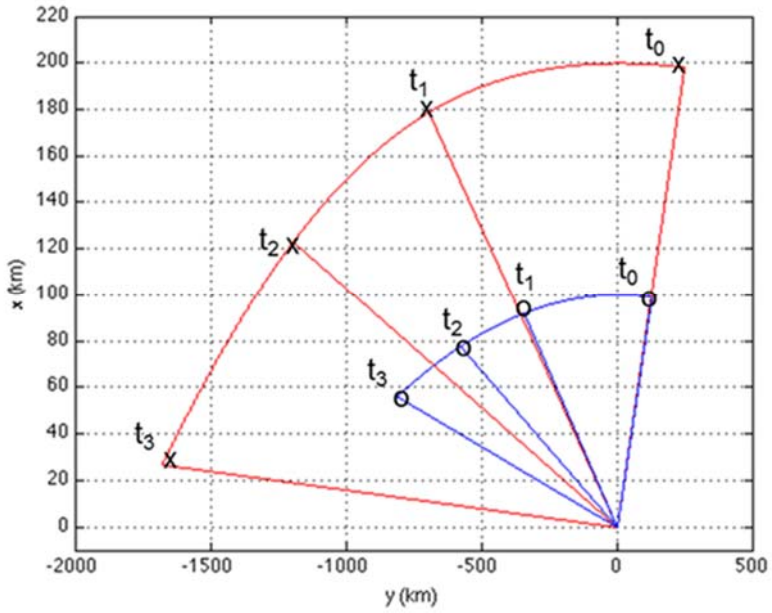


**Figure 3. Illustration of observability afforded by nonlinearity: LOS histories of two relative orbits propagated forward with nonlinear dynamics.**

.

### C. Solving the Measurement Equations

From the above discussion, we know that any IROD method based on a linear relative motion model (e.g. Clohessy-Wiltshire) will result in a set of linear homogeneous measurement equations of the form $A\bar{x}_0 = 0$, and will have no hope of determining the unique relative orbit, due to the infinite ambiguity discussed in the previous section. However, an IROD method based on a dynamic model that captures some degree of nonlinearity should have at least a possibility of success. Suppose that our IROD method utilizes the second-order relative motion solution detailed above. Note that the *x*, *y*, and *z* components of this solution can each possess up to 27 terms. Thus, each expression is of the form

$$
\begin{aligned}
x(t) &= C_1(t)x_0 + C_2(t)y_0 + \ldots + C_6(t)\dot{z}_0 + C_7(t){x_0}^2 + C_8(t)x_0y_0 + \ldots + C_{27}(t){\dot{z}_0}^2 \\
y(t) &= D_1(t)x_0 + \ldots + D_{27}(t){\dot{z}_0}^2 \\
z(t) &= E_1(t)x_0 + \ldots + E_{27}(t){\dot{z}_0}^2
\end{aligned} \tag{5}
$$

Evaluating *x(t), y(t),* and *z(t)* at measurement time $t_i$ and inserting into Eq. (2) yields

$$
\begin{aligned}
&\left[-u_z(t_i)D_1(t_i) + u_y(t_i)E_1(t_i)\right]x_0 + \ldots + \left[-u_z(t_i)D_{27}(t_i) + u_y(t_i)E_{27}(t_i)\right]{\dot{z}_0}^2 = 0 \\
&\left[u_z(t_i)C_1(t_i) - u_x(t_i)E_1(t_i)\right]x_0 + \ldots + \left[u_z(t_i)C_{27}(t_i) - u_x(t_i)E_{27}(t_i)\right]{\dot{z}_0}^2 = 0 \\
&\left[-u_y(t_i)C_1(t_i) + u_x(t_i)D_1(t_i)\right]x_0 + \ldots + \left[-u_y(t_i)C_{27}(t_i) + u_x(t_i)D_{27}(t_i)\right]{\dot{z}_0}^2 = 0
\end{aligned} \tag{6}
$$

Note that each of these equations is a second-order polynomial in six unknowns (the six initial relative states). Following the procedure of the previous subsection, if we obtain three LOS measurements, choosing two of the measurement equations at each time, this yields a "square" system of six coupled second-order polynomials in the six initial relative states. Note that these equations are *not* linear in the initial relative states, i.e. they cannot be written as $A\bar{x}_0 = 0$. Thus, if $\bar{x}_0^*$ is a solution to these equations, $\alpha\bar{x}_0^*$ is not, i.e. we have escaped the infinite ambiguity of Woffinden's dilemma by employing nonlinear relative dynamics. A similar line of reasoning could be followed if our IROD method utilizes the third-order relative motion solution, also detailed above.

The branch of applied mathematics known as numerical algebraic geometry offers multiple approaches to solving polynomial systems. In this paper, a method known as homotopy continuation is utilized, specifically, an algorithm derived and presented in Ref 14. Some discussion is in order regarding the number of solutions to the polynomial system. According to Bezout's Theorem,[15] there are $a^b$ solutions to a system of coupled polynomials, where *a* represents the order of each polynomial and *b* represents the number of polynomials (i.e. number of variables). For six 2nd-order polynomials, the number of solutions is then 64. However, these solutions are in the complex domain, i.e. it is possible that each solution may consist of one or more values with imaginary parts. There is no known theorem for how many real solutions may exist, so the best that can be said is that the *maximum* number of real solutions for a given scenario is 64. If in fact multiple real solutions exist, we have a finite ambiguity to deal with (unlike the infinite ambiguity associated with Woffinden's dilemma). While the authors have devised a clear strategy for disambiguation of the solutions, this process will not be discussed here.

.

## IV. Example Cases

In order to present and explain results as clearly as possible over numerous example cases, we first give a specific description and delineation of a simulated "case." We then describe the orbital scenarios included in the results, and the IOD and IROD methods to be utilized.

### A. Definition of a "Case"

Following are the parameters and properties that fully define a case, along with a description specific to the analysis of this paper:

- **Initial conditions**: these are specified in terms of the observer and RSO orbit elements, as detailed below.
- **Propagation scheme**: this entails the orbit propagation method used to generate simulated measurements; for this analysis, both the observer & RSO orbits are propagated with two-body dynamics.
- **Measurement times**: the LOS measurement times are detailed below.

### B. Initial Condition Scenarios

Two particular orbital scenarios are explored here, both of which are detailed in Table 1 in terms of the observer and RSO orbit elements at time $t_0 = 0$, including semimajor axis (a), eccentricity (e), inclination (i), right ascension of ascending node ($\Omega$), argument of perigee ($\omega$), and true anomaly ($\upsilon$). The first scenario was defined in Ref 9 and is thus referred to as the "Williamsburg" scenario. This scenario does not pertain to a specific mission application, rather

the conditions were chosen with some arbitrariness to effect several aspects of relative motion such as motion in all three dimensions and significant drift between the observer and RSO. This scenario is shown in Figure 4. The second scenario results in a 200 km x100 km ellipse in the LVLH *x*-*y* plane, with cross-track (*z*) motion of approximately 19 km amplitude. This scenario is referred to simply as the "200x100 Ellipse" scenario and is indicative of a rendezvous mission whereby one spacecraft is circumnavigating another in relative space. This scenario is shown in Figure 5.

**Table 1. Scenario Initial Conditions**

| Scenario | Orbit | a (km) | e | i (deg) | Ω (deg) | ω (deg) | ν (deg) |
|---|---|---|---|---|---|---|---|
| Williamsburg | Observer | 7.1000E+03 | 0.0000E+00 | 7.0000E+01 | 4.5000E+01 | 0.0000E+00 | 0.0000E+00 |
| | RSO | 7.1390E+03 | 5.4442E-03 | 7.0153E+01 | 4.5000E+01 | 3.5718E+02 | 2.8181E+00 |
| 200x100 Ellipse | Observer | 7.1000E+03 | 0.0000E+00 | 7.0000E+01 | 4.5000E+01 | 0.0000E+00 | 0.0000E+00 |
| | RSO | 7.1000E+03 | 1.4085E-02 | 7.0155E+01 | 4.5000E+01 | 1.8000E+02 | 1.7999E+02 |

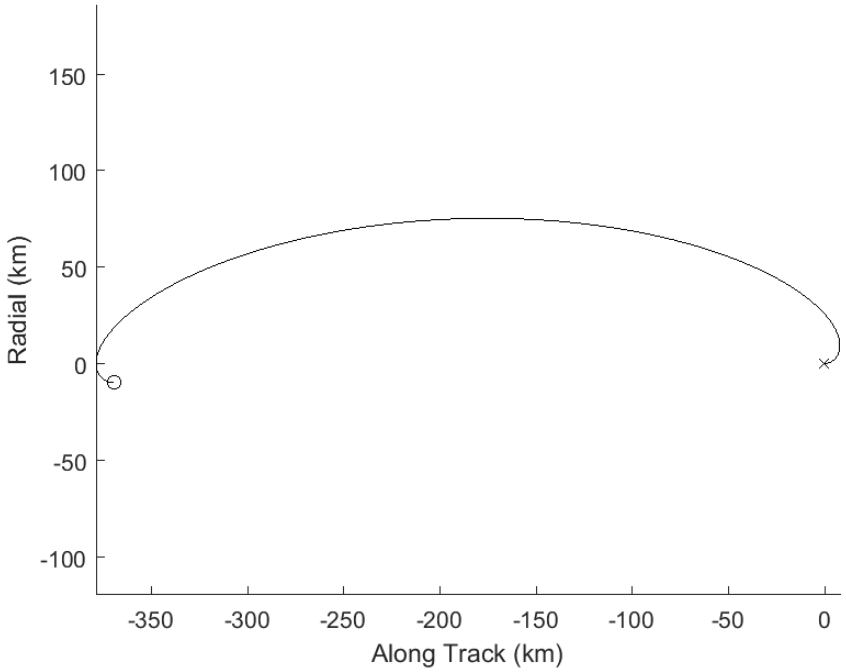


**Figure 4: True relative orbit for "Williamsburg" scenario.**

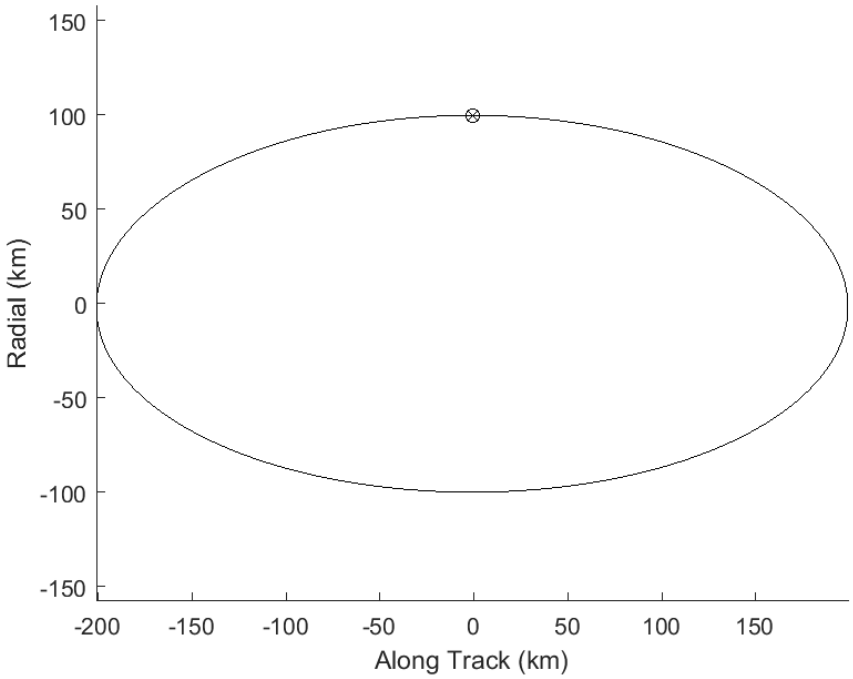


**Figure 5: True relative orbit for "200x100 ellipse" scenario.**

### C. Measurement Times

Table 2 displays the measurement times ($t_1$, $t_2$, $t_3$) chosen for the various cases. For the "Williamsburg" scenario, it was decided to hold $t_2$ constant at 2871.0844 sec (roughly ½ orbital period) and vary $t_2$ - $t_1$ (defined "$\Delta t_1$") and $t_3$ - $t_2$ (defined "$\Delta t_3$"). This resulted in six different sets of measurement times, comprising Cases I-VI in Table 2. Note that some choices of measurement times are symmetric ($\Delta t_1 = \Delta t_3$) while some are asymmetric ($\Delta t_1 \neq \Delta t_3$). For the "200x100 Ellipse" scenario, three sets of symmetric measurement times were chosen at various intervals within an orbital period, comprising Cases VII-IX in Table 2.

**Table 2. Case Introduction (All Times in sec)**

| Case | Type | t2 | Δt1 | Δt3 |
|---|---|---|---|---|
| I | Williamsburg | 2871.0844 | 2 | 2 |
| II | Williamsburg | 2871.0844 | 30 | 30 |
| III | Williamsburg | 2871.0844 | 20 | 40 |
| IV | Williamsburg | 2871.0844 | 40 | 20 |
| V | Williamsburg | 2871.0844 | 100 | 100 |
| VI | Williamsburg | 2871.0844 | 300 | 300 |
| VII | 200X100 Ellipse | 744.2327 | 50 | 50 |
| VIII | 200X100 Ellipse | 1475.2346 | 50 | 50 |
| IX | 200X100 Ellipse | 2219.4673 | 50 | 50 |

### D. Angle Error Metric

The two primary error sources in an IROD problem (or any estimation problem) are (1) model error: i.e. differences between the true observer-RSO relative motion and that predicted by the model employed; and (2) measurement error: i.e. differences between the true LOS and that measured by the sensor. For a simulated test case, the model error can be gauged to some extent by propagating the true initial relative conditions with the model (i.e. relative motion solution) to be employed in the IROD process.

Figure 6 displays the two scenarios of Table 1 propagated for one observer orbit period (displayed in the *x*-*y* plane of the observer's LVLH frame), using both two-body nonlinear dynamics as "truth" and the second-order relative motion solution detailed above. The fact that for each scenario the two curves lie essentially on top of each other seem to imply that IROD results in these scenarios will reflect little to no model error (in other words, with no measurement error, the IROD process should estimate the relative orbit nearly perfectly). However, a variable that is not considered in these plots in time; if time histories of the *x*, *y*, and *z* components of the relative motion were plotted vs time for both the two-body and second-order models, this agreement would not be as close as in Figure 6. Thus, while the second-order solution is approximating the various *x*, *y*, *z* points in each trajectory accurately, the RSO arrives at a given point (or at least some of the points) at a different time than that indicated by two-body motion (and therefore real motion). Fundamentally, this is because the instantaneous LVLH angular rate of the RSO predicted by the second-order solution does not exactly match that of two-body (and therefore real) motion. So it stands to reason that the LOS history predicted by second-order vs two-body motion will be somewhat different. Thus, because the IOD procedure involves processing LOS measurements at specific times, we see that a second-order IROD method, at least in these two scenarios, will in fact incur model error to some extent.

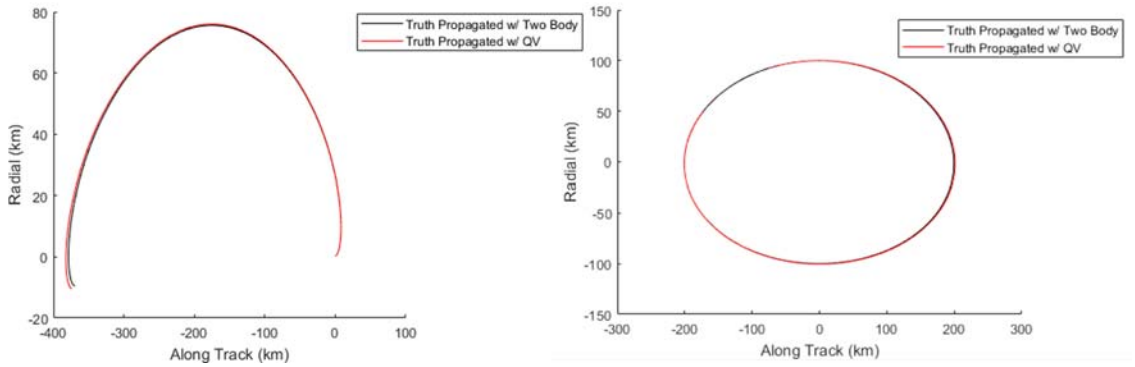


**Figure 6: True relative orbit propagated with two-body dynamics and second-order solution (Figure 6a: Williamsburg scenario, Figure 6b: 200x100 ellipse scenario).**

It is then instructive to define an "angle error" metric as the instantaneous angle between the LOS predicted by an approximate relative motion solution and that indicated by two-body motion:

$$\psi = \cos^{-1}\left(\hat{u}_r \cdot \hat{u}_r{}'\right) = \cos^{-1}\left(\frac{\bar{r}}{r} \cdot \frac{\bar{r}'}{r'}\right) \tag{7}$$

where the primed notation pertains to motion propagated with the approximate solution, and the unprimed notation pertains to motion propagated with two-body dynamics. Figure 7 displays $\psi$ for one observer orbit period for the two scenarios of Table 1. For each scenario, the red curve represents the Clohessy-Wiltshire solution as the approximate model and two-body motion as the truth model, while the blue curve represents the second-order solution as the approximate model and two-body motion as the truth model. Clearly, the second-order solution is a better approximator of LOS than Clohessy-Wiltshire, but it incurs LOS error nonetheless. Generally, this approximation will only worsen with the inclusion of measurement error.

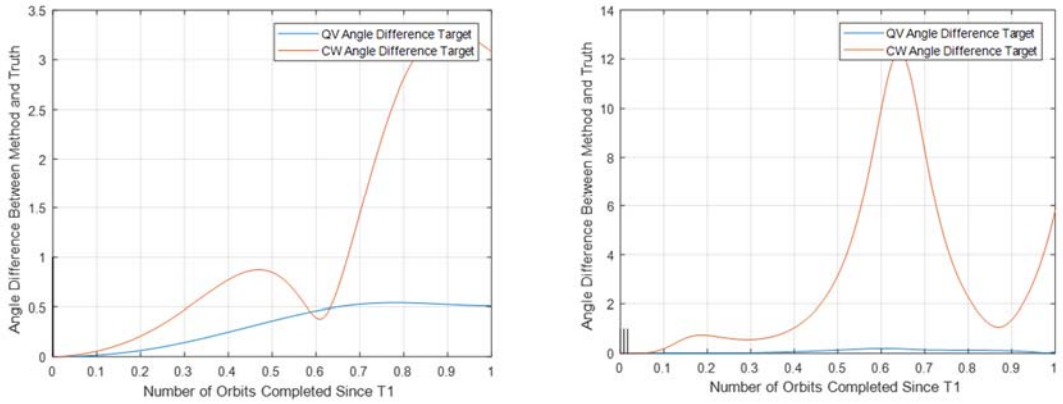


**Figure 7: Angle error metric vs time (Figure 7a: Williamsburg scenario, Figure 7b: 200x100 ellipse scenario).**

## E. Results

The first portion of results involves a comparison between the IROD method employing the second-order solution (here termed "second-order IROD") and the IROD method employing the third-order solution (here termed "third-order IROD") for each of the 9 example cases detailed in Table 1 and Table 2. Figures 8-16 each display two plots: the first plot overlays the two-body propagation of the true initial conditions (i.e. the "truth" trajectory) with the two-body propagation of the initial conditions solved by the second-order IROD method; while the second plot overlays the "truth" trajectory with the two-body propagation of the initial conditions solved by the third-order IROD method. All trajectories are propagated for one observer orbit period and displayed in the *x*-*y* plane of the observer's LVLH frame. From these results, the improved accuracy of the third-order IROD technique over that of second-order IROD is quite clear. Of these 9 cases, the most accurate second-order IROD is Case VIII, while the accuracy for all other cases is noticeably less. Whereas, third-order IROD delivers basically the same level of accuracy for all cases, and this accuracy is comparable to, if not better than, that of second-order IROD in Case VIII.

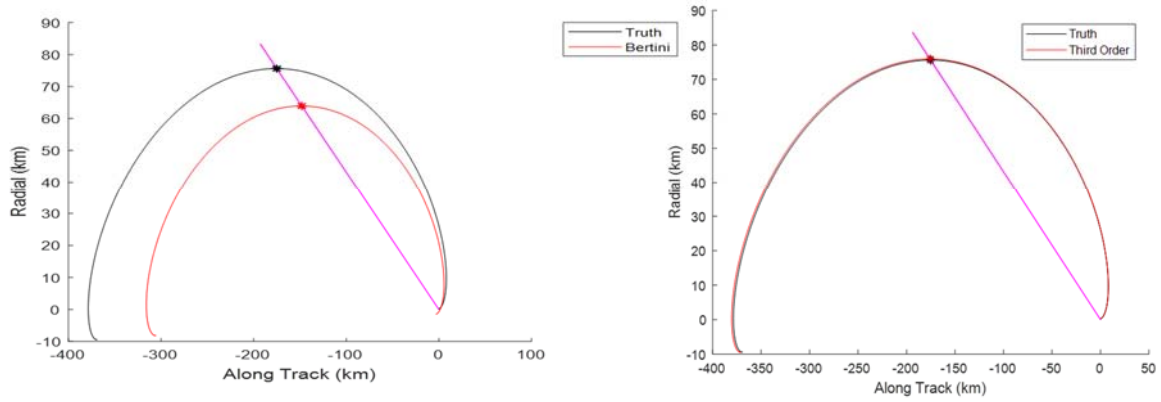


**Figure 8: Case I propagated relative orbits (Figure 8a: second-order IROD, Figure 8b: third-order IROD).**

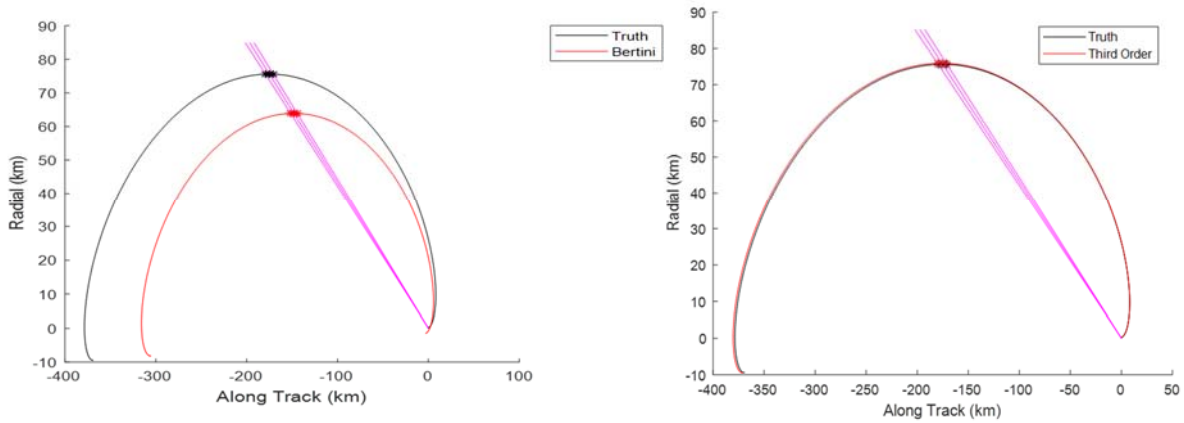


**Figure 9: Case II propagated relative orbits (Figure 9a: second-order IROD, Figure 9b: third-order IROD).**

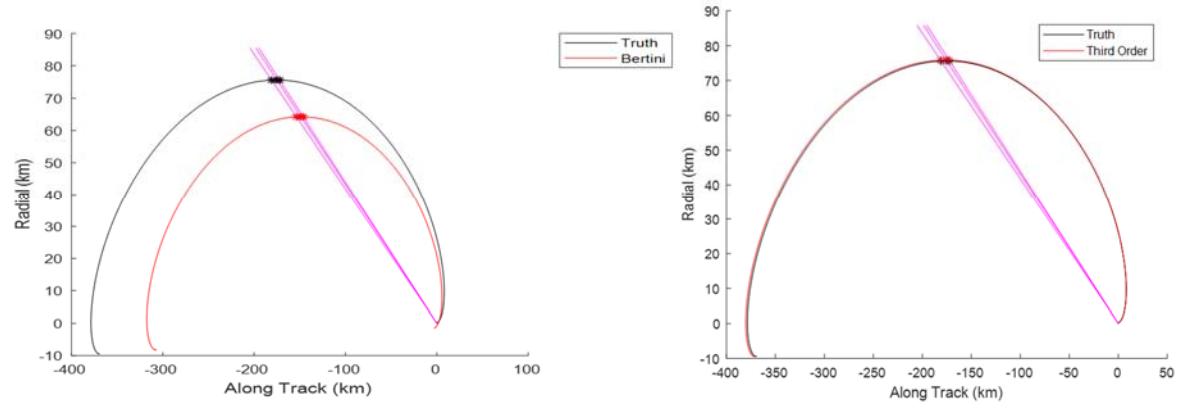


**Figure 10: Case III propagated relative orbits (Figure 10a: second-order IROD, Figure 10b: third-order IROD).**

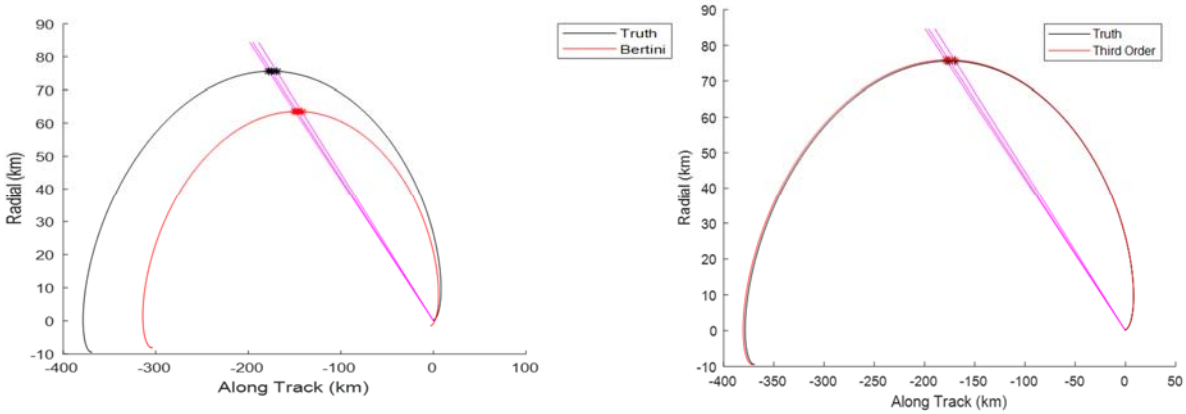


**Figure 11: Case IV propagated relative orbits (Figure 11a: second-order IROD, Figure 11b: third-order IROD).**

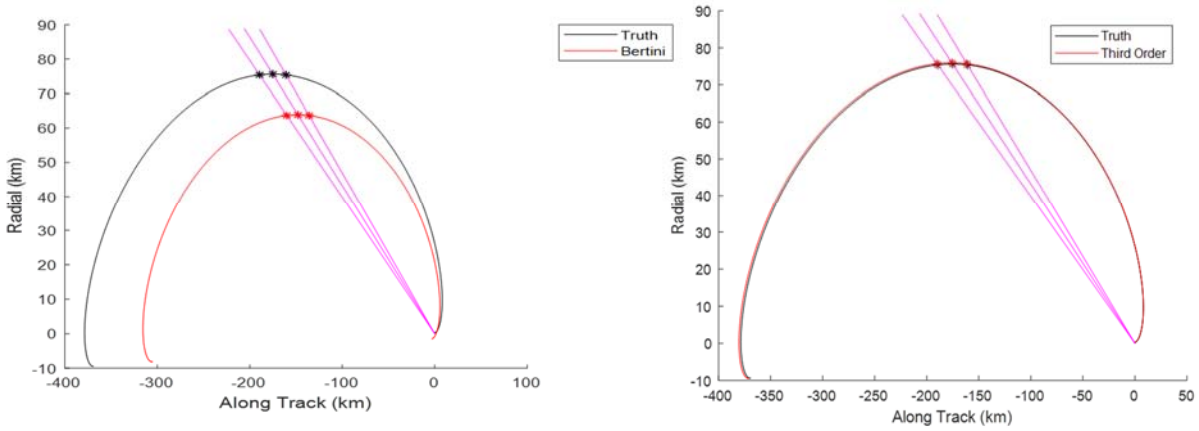


**Figure 12: Case V propagated relative orbits (Figure 12a: second-order IROD, Figure 12b: third-order IROD).**

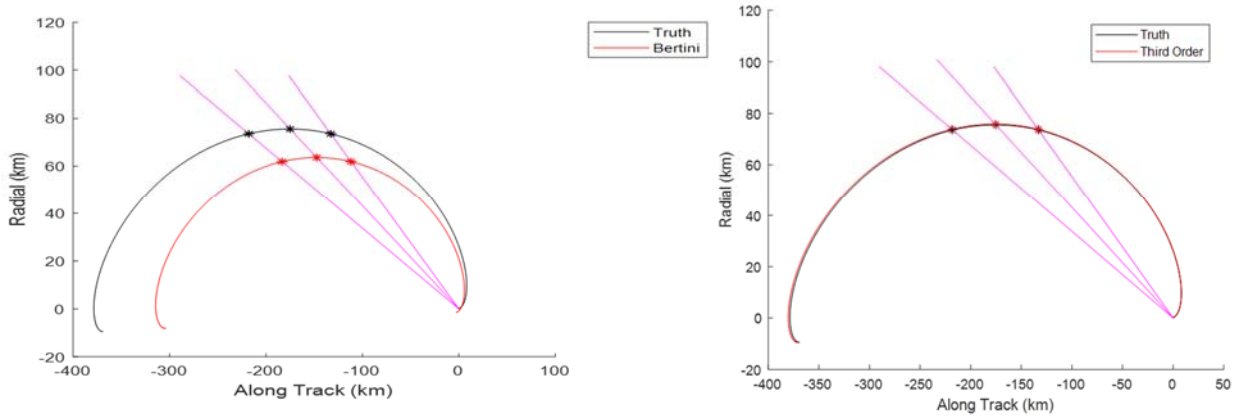


**Figure 13: Case VI propagated relative orbits (Figure 13a: second-order IROD, Figure 13b: third-order IROD).**

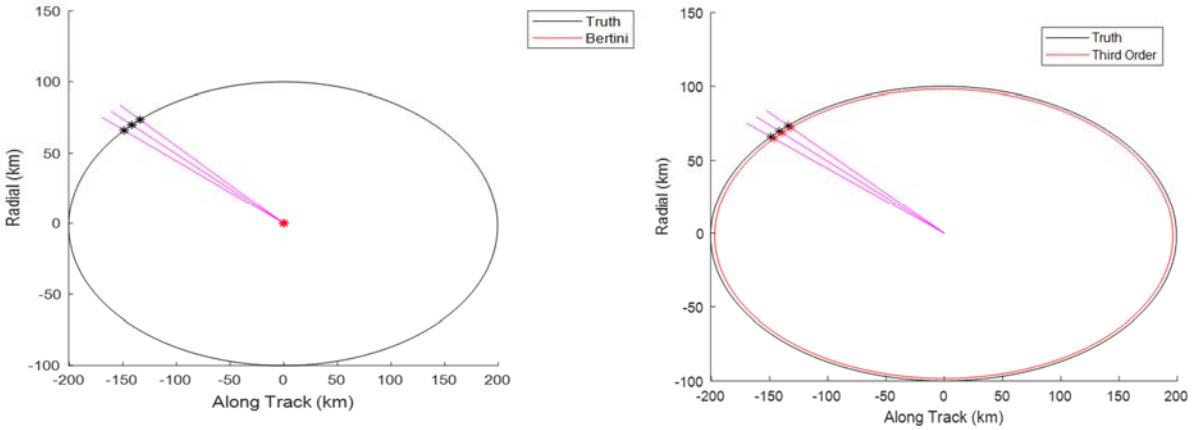


**Figure 14: Case VII propagated relative orbits (Figure 14a: second-order IROD, Figure 14b: third-order IROD).**

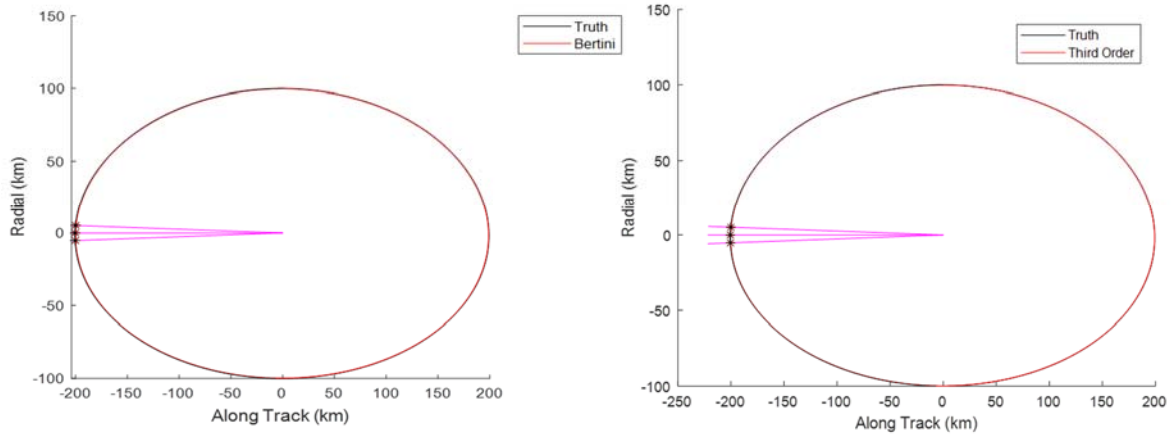


**Figure 15: Case VIII propagated relative orbits (Figure 15a: second-order IROD, Figure 15b: third-order IROD).**

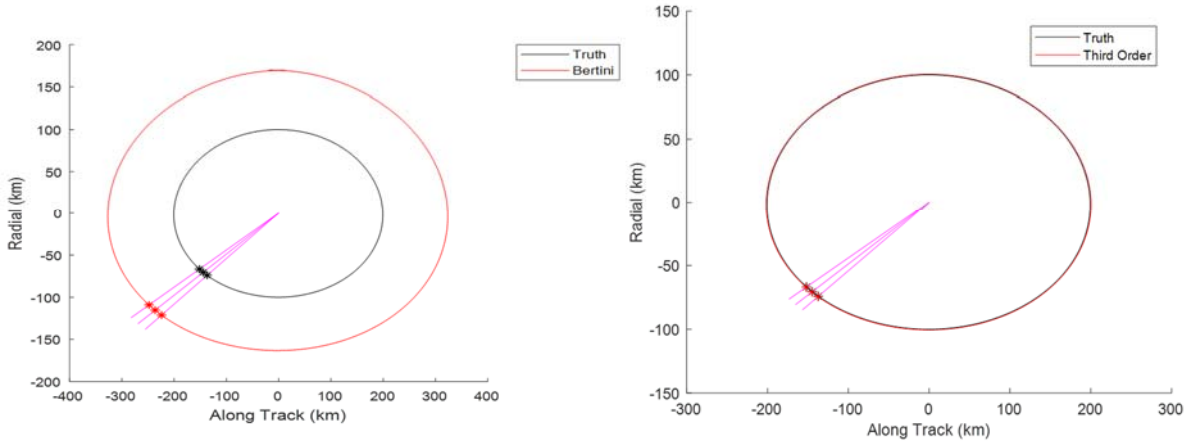


**Figure 16: Case IX propagated relative orbits (Figure 16a: second-order IROD, Figure 16b: third-order IROD).**

The second portion of results involves a comparison between second-order IROD and third-order IROD with error added to the LOS measurements. To generate each result, 10,000 Monte Carlo trials were performed with zero-mean Gaussian error added to each LOS measurement. Figure 17 shows the mean miss distance of all the trials in Cases I-VI, for Gaussian error levels from $\sigma = 10^{-8}$ rad to $\sigma = 10^{-4}$ rad. Here, miss distance is defined as the norm error between the true position vector and estimated position vector at the first measurement time.

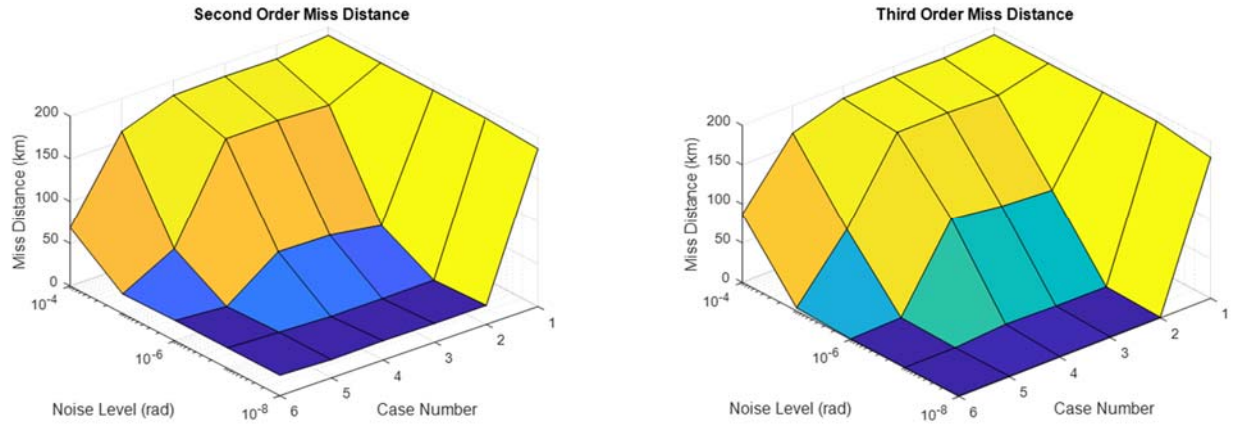


**Figure 17: Mean miss distance of all Monte Carlo trials in Cases I-VI, for varying levels of measurement error (Figure 17a: second-order IROD, Figure 17b: third-order IROD).**

For each case/error combination, the covariance matrix of the estimate was computed numerically over the 10,000 trials, and from this the position error ellipsoid was examined. The major (i.e. longest) axis of the ellipsoid in each case was in the direction from the observer to the RSO, i.e. the "range" dimension. This is to be expected, given the range observability problem of angles-only IOD. Focusing on Case VI, Table 3 shows the mean and standard deviation of range error (i.e. difference between the true position vector and estimated position vector at the first measurement time) over the 10,000 trials for each error level, as computed for both second-order and third-order IROD. Histograms of range error for both IROD methods are shown in Figures 18-19 for error levels of $\sigma = 10^{-8}$ rad and $\sigma = 10^{-5}$ rad.

**Table 3. Case Introduction (All Times in sec)**

| | | Noise Levels | | | | |
|---|---|---|---|---|---|---|
| | | 1.00E-08 | 1.00E-07 | 1.00E-06 | 1.00E-05 | 1.00E-04 |
| Second Order | μ | -23.8768 | -23.8782 | -23.8565 | -22.8696 | 68.74109 |
| | σ | 2.35E-02 | 2.35E-01 | 2.353215 | 23.71573 | 149.4587 |
| Third Order | μ | 0.621287 | 0.619221 | 0.660201 | 3.816007 | 255.4584 |
| | σ | 3.56E-02 | 3.56E-01 | 3.556668 | 40.59619 | 358.4026 |

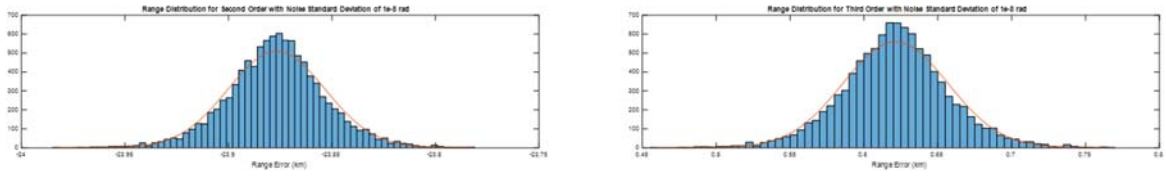

**Figure 18: Histogram of range error for $10^{-8}$ rad measurement error (Figure 18a: second-order IROD, Figure 18b: third-order IROD).**

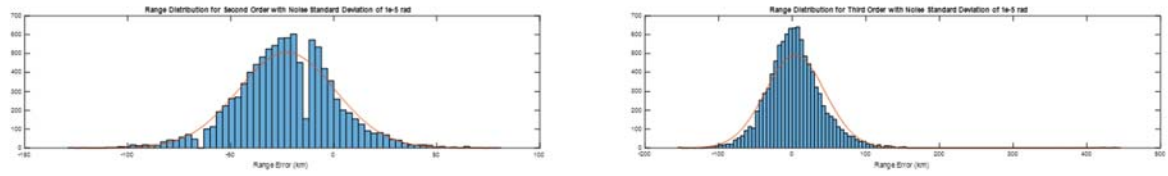

**Figure 19: Histogram of range error for $10^{-5}$ rad measurement error (Figure 19a: second-order IROD, Figure 19b: third-order IROD).**

## V. Conclusions and Future Work

This paper has explored the problem of angles-only initial orbit determination from a space-based observer using a modern approach based on relative orbital dynamics. The approach utilizes closed-form solutions for relative motion expressed as polynomials in the initial (epoch) conditions. This allows the line-of-sight measurement equations to be cast as a system of coupled polynomials, which can then be solved via mathematical techniques. The two methods explored were a method utilizing a second-order relative motion solution and one utilizing a third-order relative motion solution. Results show that the relative techniques are generally successful for the simulated examples chosen. The third-order method, while computationally more expensive, is seen to be more accurate than the second-order method. This is expected since the third-order method captures a higher degree of nonlinearity in the relative motion and therefore is able to overcome the weak observability in the size (magnitude) of the relative orbit better than the second-order method.

Planned extensions of this research include:

- Further error analysis of each method, including error introduced into the observer's orbit
- Measurement generation with higher fidelity propagation beyond two-body dynamics
- Comparing additional metrics, including computational run-time

## VI. Appendix

The following solution characterizes the motion of a "deputy" space object relative to a "chief" object in the local-vertical-local-horizontal frame of the chief's orbit, where the *x*, *y*, and *z* coordinate directions are defined in the text above. $R_0$ is the (circular) chief orbit radius and $n$ is the mean motion of the chief orbit:

$$x(t) = a_1x_0 + a_2\dot{x}_0 + a_3\dot{y}_0 + b_1x_0^2 + b_2y_0^2 + b_3\dot{x}_0^2 + b_4\dot{y}_0^2 + b_5\dot{z}_0^2 + b_6x_0y_0 + b_7x_0\dot{x}_0 + b_8x_0\dot{y}_0 + b_9y_0\dot{y}_0 + b_{10}z_0\dot{z}_0 + b_{11}z_0\dot{y}_0 + b_{12}\dot{x}_0\dot{y}_0 + c_1x_0^3 + c_2y_0^3 + c_3\dot{x}_0^3 + c_4\dot{y}_0^3 + c_5x_0^2y_0 + c_6x_0^2\dot{x}_0 + c_7x_0^2\dot{y}_0 + c_8y_0^2x_0 + c_9y_0^2\dot{x}_0 + c_{10}y_0^2\dot{y}_0 + c_{11}z_0^2x_0 + c_{12}z_0^2y_0 + c_{13}z_0^2\dot{x}_0 + c_{14}z_0^2\dot{y}_0 + c_{15}z_0^2\dot{z}_0 + c_{16}x_0\dot{x}_0^2 + c_{17}x_0\dot{y}_0^2 + c_{18}x_0\dot{z}_0^2 + c_{19}y_0\dot{x}_0^2 + c_{20}y_0\dot{y}_0^2 + c_{21}y_0\dot{z}_0^2 + c_{22}\dot{x}_0^2\dot{y}_0 + c_{23}\dot{y}_0^2\dot{x}_0 + c_{24}\dot{z}_0^2\dot{x}_0 + c_{25}\dot{z}_0^2\dot{y}_0 + c_{26}x_0y_0\dot{x}_0 + c_{27}x_0y_0\dot{y}_0 + c_{28}x_0z_0\dot{z}_0 + c_{29}x_0\dot{x}_0\dot{y}_0 + c_{30}y_0z_0\dot{z}_0 + c_{31}y_0\dot{x}_0\dot{y}_0 + c_{32}z_0\dot{x}_0\dot{z}_0 \tag{A.1}$$

where:

$$a_1 = (4 - 3\cos(nt)), \qquad a_2 = \frac{1}{n}\sin(nt), \qquad a_3 = \frac{2}{n}(1 - \cos(nt))$$

$$b_1 = \frac{3}{2R_0}(7 - 10\cos(nt) + 3\cos(2nt) + 12nt\sin(nt) - 12n^2t^2)$$

$$b_2 = \frac{3}{2R_0}(1 - \cos(nt)), \qquad b_3 = \frac{1}{2n^2R_0}(-3 + 4\cos(nt) - \cos(2nt))$$

$$b_4 = \frac{1}{2n^2R_0}(6 - 10\cos(nt) + 4\cos(2nt) + 12nt\sin(nt) - 9n^2t^2)$$

$$b_5 = \frac{1}{4n^2R_0}(3 - 4\cos(nt) + \cos(2nt))$$

$$b_6 = \frac{6}{R_0}(-\sin(nt) + nt), \qquad b_7 = \frac{3}{nR_0}(4\sin(nt) - \sin(2nt) - 4nt + 2nt\cos(nt))$$

$$b_8 = \frac{3}{nR_0}(4 - 6\cos(nt) + 2\cos(2nt) + 7nt\sin(nt) - 6n^2t^2)$$

$$b_9 = \frac{3}{nR_0}(-\sin(nt) + nt), \qquad b_{10} = \frac{1}{2nR_0}(2\sin(nt) - \sin(2nt))$$

$$b_{11} = \frac{1}{n^2R_0^2}\left(-\frac{9}{2}nt + 3nt\cos(nt) + \frac{3}{2}nt\cos(2nt) + \frac{13}{2}\sin(nt) - \frac{5}{2}\sin(2nt) - \frac{1}{2}\sin(3nt)\right)$$

$$b_{12} = \frac{1}{n^2R_0}(7\sin(nt) - 2\sin(wnt) - 6nt + 3nt\cos(nt))$$

$$c_1 = \frac{1}{R_0^2}\left(31 - 27nt^2 - \frac{545}{8}\cos(nt) - 108n^2t^2\cos(nt) + \frac{135}{2}nt\sin(2nt) + 27\cos(2nt) + \frac{81}{8}\cos(3nt) + \frac{135}{2}\,nt\sin(nt)\right)$$

$$c_2 = \frac{1}{R_0^2}(3nt - 3\sin(nt))$$

$$c_3 = \frac{1}{n^3R_0^2}\left(-3nt + \frac{3}{2}nt\cos(nt) + \frac{43}{8}\sin(nt) - \frac{5}{2}\sin(2nt) + \frac{3}{8}\sin(3nt)\right)$$

$$c_4 = \frac{1}{n^3R_0^2}(6 - 9n^2t^2 - 15\cos(nt) - 18n^2t^2\cos(nt) + 6\cos(2nt) + 3\cos(3nt) + 15nt\sin(nt) + 15nt\sin(2nt))$$

$$c_5 = \frac{1}{R_0^2}\left(\frac{21}{2}nt + 18nt\cos(nt) - 24\sin(nt) - \frac{9}{4}\sin(2nt)\right)$$

$$c_6 = \frac{1}{nR_0^2}\left(-30nt - \frac{87}{2}nt\cos(nt) + 45nt\cos(2nt) + \frac{447}{8}\sin(nt) + 36n^2t^2\sin(nt) + \frac{3}{2}\sin(2nt) - \frac{81}{8}\sin(3nt)\right)$$

$$c_7 = \frac{1}{nR_0^2}\left(57 - \frac{135}{2}n^2t^2 - \frac{513}{4}\cos(nt) - 180n^2t^2\cos(nt) + 51\cos(2nt) + \frac{81}{4}\cos(3nt) + 129nt\sin(nt) + \frac{495}{4}nt\sin(2nt)\right)$$

$$c_8 = \frac{1}{R_0^2}\left(\frac{15}{2} - 18n^2t^2 - 12\cos(nt) + \frac{9}{2}\cos(2nt) + 18\sin(nt)\right)$$

$$c_9 = \frac{1}{nR_0^2}\left(-9nt + 3nt\cos(nt) + 9\sin(nt) - \frac{3}{2}\sin(2nt)\right)$$

$$c_{10} = \frac{1}{nR_0^2}\left(6 - 9n^2t^2 - 9\cos(nt) + 3\cos(2nt) + \frac{21}{2}nt\sin(nt)\right)$$

$$c_{11} = \frac{1}{R_0^2}\left(3 - 9n^2t^2 - \frac{29}{8}\cos(nt) + \cos(2nt) - \frac{3}{8}\cos(3nt) + \frac{15}{2}nt\sin(nt) - \frac{3}{2}nt\sin(2nt)\right)$$

$$c_{12} = \frac{1}{R_0^2}\left(\frac{3}{2}nt - \sin(nt) - \frac{1}{4}\sin(2nt)\right)$$

$$c_{13} = \frac{1}{nR_0^2}\left(-3nt + \frac{3}{2nt}\cos(nt) + \frac{17}{8}\sin(nt) - \frac{1}{2}\sin(2nt) + \frac{1}{8}\sin(3nt)\right)$$

$$c_{14} = \frac{1}{nR_0^2}\left(\frac{5}{2} - \frac{9}{2}n^2t^2 - \frac{11}{4}\cos(nt) + \frac{1}{2}\cos(2nt) - \frac{1}{4}\cos(3nt) + \frac{9}{2}nt\sin(nt) - \frac{3}{4}nt\sin(2nt)\right)$$

$$c_{15} = \frac{1}{4R_0}(3 - 2\cos(nt) - \cos(2nt))$$

$$c_{16} = \frac{1}{n^2R_0^2}\left(-3 - 9n^2t^2 - \frac{37}{8}\cos(nt) + 11\cos(nt) - \frac{27}{8}\cos(3nt) + \frac{57}{2}nt\sin(nt) - \frac{15}{2}nt\sin(2nt)\right)$$

$$c_{17} = \frac{1}{n^2R_0^2}\left(33 - 45n^2t^2 - \frac{155}{2}\cos(nt) - 99n^2t^2\cos(nt) + 31\cos(2nt) + \frac{27}{2}\cos(3nt) + 78nt\sin(nt) + 75nt\sin(2nt)\right)$$

$$c_{18} = \frac{1}{n^2R_0^2}\left(\frac{9}{2} - 9n^2t^2 - \frac{67}{8}\cos(nt) + \frac{7}{2}\cos(2nt) + \frac{3}{8}\cos(3nt) + \frac{21}{2}nt\sin(nt) + \frac{3}{2}nt\sin(2nt)\right)$$

$$c_{19} = \frac{1}{n^2R_0^2}\left(\frac{15}{2}nt - 3nt\cos(nt) - 9\sin(nt) + \frac{9}{4}\sin(2nt)\right)$$

$$c_{20} = \frac{1}{n^2R_0^2}(9nt\cos(nt) - 3\sin(nt) - 3\sin(2nt))$$

$$c_{21} = \frac{1}{n^2R_0^2}\left(\frac{3}{2}nt - \frac{2\sin(nt)\,1}{4}\sin(2nt)\right)$$

$$c_{22} = \frac{1}{n^3R_0^2}\left(-\frac{9}{2}n^2t^2 - \frac{23}{4}\cos(nt) + 8\cos(2nt) - \frac{9}{4}\cos(3nt) + 15nt\sin(nt) - \frac{15}{4}nt\sin(2nt)\right)$$
$$c_{23} = \frac{1}{n^3R_0^2}\left(-9nt - 15nt\cos(nt) + 15\,nt\cos(2nt) + \frac{33}{2}\sin(nt) + 9n^2t^2\sin(nt) + 3\sin(2nt) - \frac{9}{2}\sin(3nt)\right)$$
$$c_{24} = \frac{1}{n^3R_0^2}\left(-3nt + \frac{3}{2}nt\cos(nt) + \frac{23}{8}\sin(nt) - \frac{1}{2}\sin(2nt) - \frac{1}{8}\sin(3nt)\right)$$
$$c_{25} = \tfrac{1}{n^3R_0^2}\left(2 - \tfrac{9}{2}n^2t^2 - \tfrac{17}{4}\cos(nt) + 2\cos(2nt) + \tfrac{1}{4}\cos(3nt) + 6nt\sin(nt) + \tfrac{3}{4}nt\sin(2nt)\right)$$
$$c_{26} = \frac{1}{nR_0^2}\left(-\frac{9}{2} + 18n^2t^2 + 12\cos(nt) - \frac{15}{2}\cos(2nt) - 27nt\sin(nt)\right)$$
$$c_{27} = \frac{1}{nR_0^2}(6nt + 27nt\cos(nt) - 21\sin(nt) - 6\sin(2nt))$$
$$c_{28} = \frac{1}{nR_0^2}\left(-9nt + 6nt\cos(nt) + 3nt\cos(2nt) + \frac{41}{4}\sin(nt) - 4\sin(2nt) - \frac{3}{4}\sin(3nt)\right)$$
$$c_{29} = \frac{1}{n^2R_0^2}\left(-\frac{69}{2}nt - 51nt\cos(nt) + \frac{105}{2}nt\cos(2nt) + \frac{127}{2}\sin(nt) + 36n^2t^2\sin(nt) + 5\sin(2nt) - \frac{27}{2}\sin(3nt)\right)$$
$$c_{30} = \frac{1}{nR_0^2}\left(\frac{3}{2} - 2\cos(nt) + \frac{1}{2}\cos(2nt)\right)$$
$$c_{31} = \frac{1}{n^2R_0^2}(-6 + 9n^2t^2 + 12\cos(nt) - 6\cos(2nt) - 15nt\sin(nt))$$
$$c_{32} = \frac{1}{n^2R_0^2}\left(-\frac{7}{2} + \frac{17}{4}\cos(nt) - \frac{1}{2}\cos(2nt) - \frac{1}{4}\cos(3nt)\right)$$

$$y(t) = a_1x_0 + y_0 + a_2\dot{x}_0 + a_3\dot{y}_0 + b_1x_0^2 + b_2y_0^2 + b_3z_0^2 + b_4\dot{x}_0^2 + b_5\dot{y}_0^2 + b_6\dot{z}_0^2 + b_7x_0y_0 + b_8x_0\dot{x}_0 + b_9x_0\dot{y}_0 + b_{10}y_0\dot{x}_0 + b_{11}z_0\dot{z}_0 + b_{12}\dot{x}_0\dot{y}_0 + c_1x_0^3 + c_2y_0^3 + c_3\dot{x}_0^3 + c_4\dot{y}_0^3 + c_5x_0^2y_0 + c_6x_0^2\dot{x}_0 + c_7x_0^2\dot{y}_0 + c_8y_0^2x_0 + c_9y_0^2\dot{x}_0 + c_{10}y_0^2\dot{y}_0 + c_{11}z_0^2x_0 + c_{12}z_0^2y_0 + c_{13}z_0^2\dot{x}_0 + c_{14}z_0^2\dot{y}_0 + c_{15}x_0\dot{x}_0^2 + c_{16}x_0\dot{y}_0^2 + c_{17}x_0\dot{z}_0^2 + c_{18}y_0\dot{x}_0^2 + c_{19}y_0\dot{y}_0^2 + c_{20}y_0\dot{z}_0^2 + c_{21}\dot{x}_0^2\dot{y}_0 + c_{22}\dot{x}_0 + c_{23}\dot{z}_0^2\dot{x}_0 + c_{24}\dot{z}_0^2\dot{y}_0 + c_{250}x_0y_0\dot{x}_0 + c_{26}x_0y_0\dot{y}_0 + c_{27}x_0z_0\dot{z}_0 + c_{28}x_0\dot{x}_0\dot{y}_0 + c_{29}y_0z_0\dot{z}_0 + c_{30}y_0\dot{x}_0\dot{y}_0 + c_{31}z_0\dot{x}_0\dot{z}_0 + c_{32}z_0\dot{y}_0\dot{z}_0 \tag{A.2}$$

where:

$$a_1 = (6\sin(nt) - 6nt),\ a_2 = \tfrac{2}{n}(-1 + \cos(nt)),\ a_3 = \tfrac{1}{n}(4\sin(nt) - 3nt),$$
$$b_1 = \frac{3}{4R_0}(40\sin(nt) + 3\sin(2nt) - 22nt - 24nt\cos(nt))$$
$$b_2 = \frac{2}{R_0}(\sin(nt) - nt), \qquad b_3 = \frac{1}{4R_0}(4\sin(nt) + \sin(2nt) - 6nt)$$
$$b_4 = b_6 = \frac{1}{4n^2R_0}(8\sin(nt) - \sin(2nt) - 6nt)$$
$$b_5 = \tfrac{1}{n^2R_0}(10\sin(nt) + \sin(2nt) - 6nt - 6nt\cos(nt))$$
$$b_7 = \frac{3}{R_0}(1 - \cos(nt)), \qquad b_8 = \frac{3}{2nR_0}(-5 + 4\cos(nt) + \cos(2nt) + 4nt\sin(nt))$$
$$b_9 = \frac{3}{2nR_0}(12\sin(nt) + \sin(2nt) - 7nt - 7nt\cos(nt))$$
$$b_{10} = \frac{3}{nR_0}(-\sin(nt) + nt), \qquad b_{11} = \frac{1}{2nR_0}(-3 + 4\cos(nt) - \cos(2nt))$$
$$b_{12} = \frac{1}{n^2R_0}(-3 + 2\cos(nt) + \cos(2nt) + 3nt\sin(nt))$$

$$c_1 = \frac{1}{R_0^2}\left(-35nt + 36n^3t^3 - \frac{135}{2}nt\cos(nt) - 54nt\cos(2nt) + \frac{847}{8}\sin(nt) - 108n^2t^2\sin(nt) + \frac{27}{2}\sin(2nt) + \frac{63}{8}\sin(3nt)\right)$$

$$c_2 = \frac{1}{R_0^2}\left(\frac{3}{2} - \frac{3}{2}\cos(nt)\right)$$

$$c_3 = \frac{1}{n^3R_0^2}\left(\frac{2}{3} - \frac{19}{8}\cos(nt) + 2\cos(2nt) - \frac{7}{24}\cos(3nt) + \frac{3}{2}nt\sin(nt)\right)$$

$$c_4 = \frac{1}{n^3R_0^2}\left(-7nt + \frac{9}{2}n^3t^3 - 15\,nt\cos(nt) - 12\,nt\cos(2nt) + 21\sin(nt) - 18n^2t^2\sin(nt) + 3\sin(2nt) + \frac{7}{2}\sin(3nt)\right)$$

$$c_5 = \frac{1}{R_0^2}\left(\frac{15}{2} - 18\,n^2t^2 - 12\cos(nt) + \frac{9}{2}\cos(2nt) + 18nt\sin(nt)\right)$$

$$c_6 = \frac{1}{nR_0^2}\left(-\frac{33}{2} + 36n^2t^2 + \frac{129}{8}\cos(nt) - 36n^2t^2\cos(nt) - \frac{15}{2}\cos(2nt) + \frac{63}{8}\cos(3nt) - \frac{87}{2}nt\sin(nt) + 36\,nt\sin(2nt)\right)$$

$$c_7 = \frac{1}{nR_0^2}\left(-66\,nt + 54\,n^3t^3 - 129nt\cos(nt) - 99nt\cos(2nt) + \frac{783}{4}\sin(nt) - 180n^2t^2\sin(nt) + \frac{51}{2}\sin(2nt) + \frac{63}{4}\sin(3nt)\right)$$

$$c_8 = \frac{1}{R_0^2}\left(-21.2\,nt - 18nt\cos(nt) + 24\sin(nt) + \frac{9}{4}\sin(2nt)\right)$$

$$c_9 = \frac{1}{nR_0^2}\left(-\frac{15}{4} + 3\cos(nt) + \frac{3}{4}\cos(2nt) + 3nt\sin(nt)\right)$$

$$c_{10} = \frac{1}{nR_0^2}\left(-\frac{15}{2}nt - \frac{21}{2}nt\cos(nt) + 15\sin(nt) + \frac{3}{2}\sin(2nt)\right)$$

$$c_{11} = \frac{1}{R_0^2}\left(-3nt - \frac{15}{2}nt\cos(nt) - \frac{3}{2}nt\cos(2nt) + \frac{67}{8}\sin(nt) + \frac{5}{4}\sin(2nt) + \frac{3}{8}\sin(3nt)\right)$$

$$c_{12} = \frac{1}{R_0^2}\left(\frac{3}{4} - \frac{1}{2}\cos(nt) - \frac{1}{4}\cos(2nt)\right)$$

$$c_{13} = \frac{1}{nR_0^2}\left(-\frac{5}{4} + \frac{7}{8}\cos(nt) + \frac{1}{4}\cos(2nt) + \frac{1}{8}\cos(3nt) + \frac{3}{2}nt\sin(nt)\right)$$

$$c_{14} = \frac{1}{nR_0^2}\left(-\frac{15}{4}nt - \frac{9}{2}nt\cos(nt) - \frac{3}{4}nt\cos(2nt) + \frac{25}{4}\sin(nt) + \sin(2nt) + \frac{1}{4}\sin(3nt)\right)$$

$$c_{15} = \frac{1}{n^2R_0^2}\left(6nt - \frac{57}{2}nt\cos(nt) + 6\,nt\cos(2nt) + \frac{35}{8}\sin(nt) + 10\sin(2nt) - \frac{21}{8}\sin(3nt)\right)$$

$$c_{16} = \frac{1}{n^2R_0^2}\left(-39nt + 27n^3t^3 - 78nt\cos(nt) - 60nt\cos(wnt) + \frac{229}{2}\sin(nt) - 99n^2t^2\sin(nt) + \frac{31}{2}\sin(2nt) + \frac{21}{2}\sin(3nt)\right)$$

$$c_{17} = \frac{1}{n^2R_0^2}\left(-\frac{15}{2}nt - \frac{21}{2}nt\cos(nt) + \frac{3}{2}nt\cos(2nt) + \frac{125}{8}\sin(nt) + \sin(2nt) - 38\sin(3nt)\right)$$

$$c_{18} = \frac{1}{n^2R_0^2}\left(\frac{3}{2} - \frac{3}{2}\cos(2nt) - 3nt\sin(nt)\right)$$

$$c_{19} = \frac{1}{n^2R_0^2}\left(-\frac{9}{2}n^2t^2 - 3\cos(nt) + 3\cos(2nt) + 9nt\sin(nt)\right)$$

$$c_{20} = \frac{1}{n^2R_0^2}\left(\frac{3}{4} - \cos(nt) + \frac{1}{4}\cos(2nt)\right)$$

$$c_{21} = \frac{1}{n^3R_0^2}\left(3nt - 15nt\cos(nt) + 3nt\cos(2nt) + \frac{1}{4}\sin(nt) + 7\sin(2nt) - \frac{7}{4}\sin(3nt)\right)$$

$$c_{22} = \frac{1}{n^3 R_0^2}\left(-\frac{7}{2} + 9n^2t^2 + \frac{9}{2}\cos(nt) - 9n^2t^2\cos(nt) - \frac{9}{2}\cos(2nt) + \frac{7}{2}\cos(3nt) - 15nt\sin(nt) + 12nt\sin(2nt)\right)$$

$$c_{23} = \frac{1}{n^3 R_0^2}\left(-1 + \frac{1}{8}\cos(nt) + \cos(2nt) - \frac{1}{8}\cos(3nt) + \frac{3}{2}nt\sin(nt)\right)$$

$$c_{24} = \frac{1}{n^3 R_0^2}\left(-\frac{15}{4}nt - 6nt\cos(nt) + \frac{3}{4}nt\cos(2nt) + \frac{31}{4}\sin(nt) + \sin(2nt) - \frac{1}{4}\sin(3nt)\right)$$

$$c_{25} = \frac{1}{nR_0^2}(6nt + 27nt\cos(nt) - 21\sin(nt) - 6\sin(2nt))$$

$$c_{26} = \frac{1}{nR_0^2}\left(\frac{9}{2} - 18n^2t^2 - 12\cos(nt) + \frac{15}{2}\cos(2nt) + 27nt\sin(nt)\right)$$

$$c_{27} = \frac{1}{nR_0^2}\left(-\frac{9}{2} + \frac{19}{4}\cos(nt) + \frac{1}{2}\cos(2nt) - \frac{3}{4}\cos(3nt) + 6\,nt\sin(nt) - 3nt\sin(2nt)\right)$$

$$c_{28} = \frac{1}{n^2 R_0^2}\left(-\frac{33}{2} + 36n^2t^2 + \frac{35}{2}\cos(nt) - 36n^2t^2\cos(nt) - \frac{23}{2}\cos(2nt) + \frac{21}{2}\cos(3nt) - 51nt\sin(nt) + 42nt\sin(2nt)\right)$$

$$c_{29} = \frac{1}{nR_0^2}\left(\sin(nt) - \frac{1}{2}\sin(2nt)\right)$$

$$c_{30} = \frac{1}{n^2 R_0^2}\left(3nt + 15\,nt\cos(nt) - 9\sin(nt) - \frac{9}{2}\sin(2nt)\right)$$

$$c_{31} = \frac{1}{n^2 R_0^2}\left(\frac{5}{4}\sin(nt) - \sin(2nt) + \frac{1}{4}\sin(3nt)\right)$$

$$c_{32} = \frac{1}{n^2 R_0^2}\left(-\frac{5}{2} + \frac{5}{2}\cos(nt) + \frac{1}{2}\cos(2nt) - \frac{1}{2}\cos(3nt) + 3nt\sin(nt) - \frac{3}{2}nt\sin(2nt)\right)$$

$$z(t) = a_1 z_0 + a_2\dot{z} + b_1 x_0 z_0 + b_2 x_0\dot{z}_0 + b_3 z_0\dot{x}_0 + b_4 z_0\dot{y}_0 + b_5\dot{x}_0\dot{z}_0 + b_6\dot{y}_0\dot{z}_0 + c_1 z_0^3 + c_2\dot{z}_0^3 + c_3 x_0^2 z_0 + c_4 x_0^2\dot{z}_0 + c_5 y_0^2 z_0 + c_6 y_0^2\dot{z}_0 + c_7 z_0^2\dot{z}_0 + c_8 z_0\dot{x}_0^2 + c_9 z_0\dot{y}_0^2 + c_{10} z_0\dot{z}_0^2 + c_{11}\dot{x}_0^2\dot{z}_0 + c_{12}\dot{y}_0^2\dot{z}_0 + c_{13} x_0 z_0\dot{x}_0 + c_{14} x_0 z_0\dot{y}_0 + c_{15} x_0\dot{x}_0\dot{z}_0 + c_{16} x_0\dot{y}_0\dot{z}_0 + c_{17} y_0 z_0\dot{x}_0 + c_{18} y_0 z_0\dot{y}_0 + c_{19} y_0\dot{x}_0\dot{z}_0 + c_{20} y_0\dot{y}_0\dot{z}_0 + c_{21} z_0\dot{x}_0\dot{y}_0 + c_{22}\dot{x}_0\dot{y}_0\dot{z}_0 \quad (A.3)$$

where:

$$a_1 = \cos(nt), \qquad a_2 = \frac{1}{n}\sin(nt)$$

$$b_1 = \frac{3}{2R_0}(-3 + 2\cos(nt) + \cos(2nt) + 4nt\sin(nt))$$

$$b_2 = \frac{3}{2nR_0}(2\sin(nt) + \sin(2nt) - 4nt\cos(nt))$$

$$b_3 = \frac{1}{2nR_0}(2\sin(nt) - \sin(2nt)), \qquad b_4 = \frac{1}{nR_0}(-3 + 2\cos(nt) + \cos(2nt) + 3nt\sin(nt))$$

$$b_5 = \frac{1}{2n^2 R_0}(3 - 4\cos(nt) + \cos(2nt)), \; b_6 = \frac{1}{n^2 R_0}(\sin(nt) + \sin(2nt) - 3nt\cos(nt))$$

$$c_1 = \frac{1}{R_0^2}\left(-\frac{3}{4} + \frac{1}{2}\cos(nt) + \frac{1}{4}\cos(2nt) + \frac{3}{2}nt\sin(nt)\right)$$

$$c_2 = \frac{1}{n^3 R_0^2}\left(-\frac{3}{2}nt\cos(nt) + \frac{1}{2}\sin(nt) + \frac{1}{2}\sin(2nt)\right)$$

$$c_3 = \frac{1}{R_0^2}\left(-18 + \frac{69}{8}\cos(nt) - 18n^2t^2\cos(nt) + 6\cos(nt) + \frac{27}{8}\cos(3nt) + \frac{21}{2}nt\sin(nt) + 18nt\sin(2nt)\right)$$

$$c_4 = \frac{1}{nR_0^2}\left(-\frac{21}{2}nt\cos(nt) - 18\,nt\cos(2nt) + \frac{51}{8}\sin(nt) - 18n^2t^2\sin(nt) + 6\sin(2nt) + \frac{27}{8}\sin(3nt)\right)$$

$$c_5 = \frac{1}{R_0^2}\left(-\frac{9}{4} + \frac{3}{2}\cos(nt) + \frac{3}{4}\cos(2nt) + 3nt\sin(nt)\right)$$

$$c_6 = \frac{1}{nR_0^2}\left(-3nt\cos(nt) + \frac{3}{2}\sin(nt) + \frac{3}{4}\sin(2nt)\right)$$
$$c_7 = \frac{1}{nR_0^2}\left(-\frac{3}{2}nt\cos(nt) + 2\sin(nt) - \frac{1}{4}\sin(2nt)\right)$$
$$c_8 = \frac{1}{n^2R_0^2}\left(-\frac{3}{2} + \frac{3}{8}\cos(nt) + \frac{3}{2}\cos(2nt) - \frac{3}{8}\cos(3nt) + \frac{3}{2}nt\sin(nt)\right)$$
$$c_9 = \frac{1}{n^2R_0^2}\left(-\frac{15}{2} + \frac{7}{2}\cos(nt) - \frac{9}{2}n^2t^2\cos(nt) + \frac{5}{2}\cos(2nt) + \frac{3}{2}\cos(3nt) + 6nt\sin(nt) + 6nt\sin(2nt)\right)$$
$$c_{10} = \frac{1}{n^2R_0^2}\left(-\cos(nt) + \cos(2nt) + \frac{3}{2}nt\sin(nt)\right)$$
$$c_{11} = \frac{1}{n^3R_0^2}\left(-\frac{3}{2}nt\cos(nt) - \frac{11}{8}\sin(nt) + 2\sin(2nt) - \frac{3}{8}\sin(3nt)\right)$$
$$c_{12} = \frac{1}{n^3R_0^2}\left(-3nt\cos(nt) - 6nt\cos(2nt) + \frac{3}{2}\sin(nt) - \frac{9}{2}n^2t^2\sin(nt) + \frac{3}{2}\sin(2nt) + \frac{3}{2}\sin(3nt)\right)$$
$$c_{13} = \frac{1}{nR_0^2}\left(-6nt\cos(nt) + 6nt\cos(2nt) + \frac{11}{4}\sin(nt) + 2\sin(2nt) - \frac{9}{4}\sin(3nt)\right)$$
$$c_{14} = \frac{1}{nR_0^2}\left(-24 + \frac{23}{2}\cos(nt) - 18n^2t^2\cos(nt) + 8\cos(2nt) + \frac{9}{2}\cos(3nt) + 18\,nt\sin(nt) + 21\sin(2nt)\right)$$
$$c_{15} = \frac{1}{n^2R_0^2}\left(\frac{15}{2} - \frac{25}{4}\cos(nt) - \frac{7}{2}\cos(2nt) + \frac{9}{4}\cos(3nt) - 12nt\sin(nt) + 6nt\sin(2nt)\right)$$
$$c_{16} = \frac{1}{n^2R_0^2}\left(-12nt\cos(nt) - 21nt\cos(2nt) + \frac{13}{2}\sin(nt) - 18n^2t^2\sin(nt) + \frac{13}{2}\sin(2nt) + \frac{9}{2}\sin(3nt)\right)$$
$$c_{17} = \frac{1}{nR_0^2}(3 - 2\cos(nt) - \cos(2nt) - 3nt\sin(nt))$$
$$c_{18} = \frac{1}{nR_0^2}\left(\sin(nt) - \frac{1}{2}\sin(2nt)\right)$$
$$c_{19} = \frac{1}{n^2R_0^2}(3nt\cos(nt) - \sin(nt) - \sin(2nt))$$
$$c_{20} = \frac{1}{n^2R_0^2}\left(\frac{3}{2} - 2\cos(nt) + \frac{1}{2}\cos(2nt)\right)$$
$$c_{21} = \frac{1}{n^2R_0^2}\left(-3nt\cos(nt) + 3nt\cos(2nt) + \frac{3}{2}\sin(nt) + \frac{3}{2}\sin(2nt) - \frac{3}{2}\sin(3nt)\right)$$
$$c_{22} = \frac{1}{n^3R_0^2}\left(3 - \frac{3}{2}\cos(nt) - 3\cos(2nt) + \frac{3}{2}\cos(3nt) - 6nt\sin(nt) + 3nt\sin(2nt)\right)$$

## VII. References


1. P. R. Escobal, Methods of Orbit Determination. Wiley, New York, 1965. Ch. 7
2. G. Der, "Angles-Only Algorithms for Initial Orbit Determination Revisited," AAS/AIAA Astrodynamics Specialist Conference, Vail, Colorado, August 2015, AAS Paper 15-539
3. B. Wie and J. Ahm, "On Selecting the Correct Root of Angles-Only Initial Orbit Determination Equations of Laplace and Gauss," AAS/AIAA Space Flight Mechanics Meeting, Napa, California, February 2016, AAS Paper 16-344
4. Tschauner, J. F. A., and Hempel, P. R., "Rendezvous zu einem in elliptischer Bahn umlaufenden Ziel," Astronautica Acta, Vol. 11, No. 2, 1965, pp. 104–109
5. Clohessy, W. H., and Wiltshire, R. S., "Terminal Guidance System for Satellite Navigation." Journal of Aerospace Sciences 29, pp. 653-658, 1960
6. London, H. S., "Second Approximation to the Solution of the Rendezvous Equations," AIAA Journal, Vol. 1, No. 7, 1963, pp. 1691–1693
7. Anthony, M. L. and Sasaki, F. T., "Rendezvous Problem for Nearly Circular Orbits," AIAA Journal, Vol. 3, No. 7, 1965, pp. 1666–1673

8. Newman, B. A., and Lovell, T. A., “Second Order Nonlinear Boundary Value Solution for Relative Motion Using Volterra Theory,” AAS Paper 13-470, presented at the AAS/AIAA Space Flight Mechanics Meeting, Kauai, HI, Feb 10-14, 2013
9. Newman, B. A., Lovell, T. A., Pratt, E., and Duncan, E., “Quadratic Hexa-Dimensional Solution for Relative Orbit Determination – Revisited," AAS Paper 15-398, presented at the AAS/AIAA Space Flight Mechanics Meeting, Williamsburg, Virginia, January 2015
10. Sinclair, A. J., Lovell, T. A., Horneman, K. R., Harris, A. T., Sizemore, A. E., “Relative-Motion Approach for Differential Correction in Orbit Determination”, AAS Paper 17-327, presented at the AAS/AIAA Space Flight Mechanics Meeting, San Antonio, Texas, 9-13 February 2017
11. Horneman, K. R., Sizemore, A. E., Morton, B. W., Lovell, T. A., Newman, B. A., and Sinclair, A. J., “Angles-Only Initial Orbit Determination: Comparison of Relative Dynamics and Inertial Dynamics Approaches,” IWSCFF Paper 17-73, presented at the International Workshop on Spacecraft Formation Flying, 19-21 June 2017
12. Butcher, Lovell, and Harris, “Third Order Cartesian Relative Motion Perturbation Solutions for Slightly Eccentric Chief Orbits”, AAS Paper 16-496, presented at the AAS/AIAA Space Flight Mechanics Meeting, Napa, California, 14-18 February 2016
13. Woffinden, D., Angles-Only Navigation for Autonomous Orbital Rendezvous. PhD thesis, Utah State University, Logan, Utah, Aug. 2008Newman, Lovell, Pratt, and Duncan, “Quadratic Hexa-Dimensional Solution for Relative Orbit Determination - Revisit-ed,” AAS Paper 15-398, presented at the AAS/AIAA Space Flight Mechanics Meeting, Williamsburg, VA, Jan 11-15, 2015
14. Bates, D. J., Hauenstein, J. D., Sommese, A. J., and Wampler, C. W. Numerically solving polynomial systems with Bertini. SIAM, 2013
15. Kirwan, F., Complex Algebraic Curves, Cambridge University Press, Cambridge, England, 1992